J. Astrophys. Astr. (2018) 39:10
https://doi.org/10.1007/s12036-017-9500-7

Study of magnetized accretion flow with cooling processes

KULDEEP SINGH[1,2] and INDRANIL CHATTOPADHYAY[1,*]

[1]Aryabhatta Research Institute of Observational Sciences (ARIES), Manora Peak, Nainital 263 002, India.
[2]University of Delhi, South Campus, Delhi 110 021, India.
*Corresponding author. E-mail: indra@aries.res.in

MS received 21 August 2017; accepted 25 September 2017; published online 9 February 2018

Abstract. We have studied shock in magnetized accretion flow/funnel flow in case of neutron star with bremsstrahlung cooling and cyclotron cooling. All accretion solutions terminate with a shock close to the neutron star surface, but at some regions of the parameter space, it also harbours a second shock away from the star surface. We have found that cyclotron cooling is necessary for correct accretion solutions which match the surface boundary conditions.

Keywords. Neutron star—magnetohydrodynamics—funnel flow.

1. Introduction

Neutron stars (NS) are very fascinating objects because they have strong magnetic and gravitation fields. Neutron stars accrete rotating matter from the companion, in the form of a disc, up to the distance where $B^2/8\pi \sim (p, \rho v^2)$. Within this radius, the magnetic field is so strong that it channels all the matter along it and accretes in the form of accretion curtains. These accretion curtains fall on the polar caps of the NS which is also known as funnel flow/magnetized accretion. There are many existing models (e.g. Pringle & Rees 1972; Lamb *et al*. 1973; Davidson & Ostriker 1973; Ghosh & Lamb 1979; Lovelace *et al*. 1985, 1986; Camenzind 1990; Paatz & Camenzind 1996; Ostriker & Shu 1995; Li & Wilson 1999) which address some of the issues of magnetized accretion flow, for e.g., inner radius of accretion disc, transition zone and radiations from polar caps. However, most of the models are qualitative descriptions of the magnetized accretion flow and related phenomena. Koldoba *et al*. (2002) solved the equations of motion of matter falling along the funnel in strong field approximation and in Newtonian gravity. But accretion solutions from their model did not satisfy the surface boundary conditions, i.e., velocity near the star surface $\sim 0.1c$. Karino *et al*. (2008) studied the possibility of shock formation in magnetized accretion flow onto NS following Koldoba *et al*. (2002), but they considered only those solutions which satisfied the inner boundary condition on the NS surface. In Karino *et al*. (2008), accretion solution only satisfy boundary conditions when shock location is very far from the NS surface, which is not generally the case. Also in these models, they used Newtonian gravity without any cooling mechanism. We know that Newtonian gravity fails when it is very close to compact objects like NS and cooling should be important in accretion column of a NS. In this paper, we have studied magnetized accretion flow/funnel flow, by extending Koldoba *et al*. (2002) and Karino *et al*. (2008) by considering Paczyński–Wiita pseudo-potential to mimic strong gravity and cooling processes (bremsstrahlung and cyclotron cooling).

In section 2, we present the general magneto hydrodynamic (MHD) equations, assumptions, cooling processes and shock conditions. The methodology to find the accretion solution is explained in section 3. The parameter space and accretion flow solutions for rotation period 1 s and 10 ms are discussed in section 4 and we give the concluding remarks in section 5.

2. Governing equations and assumptions

2.1 *Basic equations*

In this study we have used ideal MHD equations. There are five conserved quantities which can be obtained from MHD equations by integrating them along the field

lines with steady state and axis-symmetry assumption. These field lines are labeled by stream function of the magnetic field and it remains constant on a field line (Ustyugova *et al.* 1999; Heinemann & Olbert 1978). The MHD equations for steady state are

$$\nabla \cdot (\rho \mathbf{v}) = 0, \tag{1}$$

$$\nabla \cdot \mathbf{B} = 0, \tag{2}$$

$$\nabla \times (\mathbf{v} \times \mathbf{B}) = 0, \tag{3}$$

$$(\rho \mathbf{v} \cdot \nabla)\mathbf{v} = -\nabla p + \frac{1}{c}(\mathbf{J} \times \mathbf{B}) + \Phi'(r)\hat{\mathbf{r}}. \tag{4}$$

Here, ρ is the mass density, $\mathbf{v}$ is the flow velocity, $\mathbf{B}$ is the magnetic field, p is the fluid pressure, Φ is the gravitational potential, r is the radial coordinate and $\hat{\mathbf{r}}$ is the unit vector along r. The velocity and magnetic field have poloidal and azimuthal components and are given by $\mathbf{v} \equiv (v_\mathrm{p}, 0, v_\phi)$ and $\mathbf{B} \equiv (B_\mathrm{p}, 0, B_\phi)$. The angular velocity of matter is related to its azimuthal velocity as $\omega = v_\phi / r$. In addition, the first law of thermodynamics or the conservation of energy equation is given by

$$\rho v_\mathrm{p} \left[\frac{\mathrm{d}(e/\rho)}{\mathrm{d}r} - \frac{p}{\rho^2} \frac{\mathrm{d}\rho}{\mathrm{d}x} \right] = Q_\mathrm{br} + Q_\mathrm{cycl}, \tag{5}$$

where $e = p/(\gamma - 1)$ is the internal energy density and Q_br and Q_cycl are the bremsstrahlung and cyclotron cooling terms. The cooling terms are given by the bremsstrahlung cooling

$$Q_\mathrm{br} = \Lambda_\mathrm{br} \rho^2 T_\mathrm{e}^{1/2}, \tag{6}$$

and cyclotron cooling is given by

$$Q_\mathrm{cycl} = \Lambda_\mathrm{cycl} \left(\frac{A_\mathrm{p}}{10^{15}\ \mathrm{cm}} \right)^{-17/40} \left(\frac{B_\mathrm{p}}{10^7\ \mathrm{G}} \right)^{57/20} \times \left(\frac{\rho}{4 \times 10^{-8}\ \mathrm{g/cm^3}} \right)^{3/20} \left(\frac{T_\mathrm{e}}{10^8\ \mathrm{K}} \right). \tag{7}$$

In the above, $\Lambda_\mathrm{br} \sim 5 \times 10^{20}\ \mathrm{erg\,cm^{-3}\,g^{-2}\,K^{-1/2}\,s^{-1}}$ and $\Lambda_\mathrm{cycl} \sim 1.2 \times 10^8\ \mathrm{erg\,cm^{-3}\,s^{-1}}$ (Busschaert *et al.* 2015). T_e is the electron temperature and is, in general, smaller than the proton temperature, and we approximate it as $T_\mathrm{e} = \sqrt{m_\mathrm{e}/m_\mathrm{p}}T$ (Chattopadhyay & Chakrabarti 2002; Das & Chattopadhyay 2008).

The differential equations (1)–(5), when integrated, admit constants of motion and are given by

(i) From the continuity equation (1), we obtain

$$\rho v_\mathrm{p} A_\mathrm{p} = \text{constant} = \dot{M} = \text{mass inflow rate}, \tag{8}$$

where A_p is the area of cross-section of the flux tube.
(ii) Equation (2) gives the magnetic flux conservation,

$$B_\mathrm{p} A_\mathrm{p} = \text{constant}, \tag{9}$$

and if we combine equations (8) and (9), we can write v_p as a function of ρ and B_p,

$$v_\mathrm{p} = \frac{\kappa(\Psi)}{4\pi\rho} B_\mathrm{p}, \tag{10}$$

where κ is ratio of the mass flux to the magnetic flux and Ψ is the stream function.
(iii) From Faraday equation (3),

$$\Omega(\Psi) = \omega - \frac{\kappa(\Psi) B_\phi}{4\pi\rho\varpi} = \text{constant}. \tag{11}$$

Here, Ω is the angular velocity of the magnetic field, $\varpi = r \sin\theta$, where θ is the polar angle.
(iv) The azimuthal component of momentum balance equation (4) gives the total angular momentum (Λ) conservation which is the sum of the angular momentum of matter and angular momentum associated with the magnetic field of the star,

$$\Lambda(\Psi) = \omega\varpi^2 - \frac{B_\phi \varpi}{\kappa(\Psi)} = \text{constant}. \tag{12}$$

(v) By integrating radial component of momentum balance equation (4), with the help of other equations, we obtain the conservation of total energy (E) along the field lines,

$$E(\Psi) = \frac{1}{2}v_\mathrm{p}^2 + \frac{1}{2}(\omega - \Omega)^2\varpi^2 + h + \Phi(r) - \frac{\Omega^2\varpi^2}{2} - \int \frac{Q\mathrm{d}r}{\rho v_\mathrm{p}} = \text{constant}, \tag{13}$$

where $\Phi(r) = -\frac{GM}{r - r_\mathrm{g}}$ is Paczyński–Wiita potential, $r_\mathrm{g} = \frac{2GM}{c^2}$ and Q is the total cooling which is given by

$$Q = Q_\mathrm{br} + Q_\mathrm{cycl}.$$

2.2 *Assumptions*

We know that NSs have very strong magnetic field, so we can assume that $B_\mathrm{p}^2/8\pi \gg (p,\ \rho v^2)$ (see Koldoba *et al.* 2002). It means that dynamics of accretion process is controlled by the magnetic field, which also implies that the flow is sub-Alfvénic, i.e. $v_\mathrm{p}/v_\mathrm{pA} \ll 1$ or $\rho_\mathrm{A}/\rho \ll 1$, where $v_\mathrm{pA} = B_\mathrm{pA}/(4\pi\rho_\mathrm{A})$ is Alfvén speed and ρ_A is mass density at the Alfvén radius. We assume that the star has dipole-like magnetic field whose magnetic moment (μ) is aligned with the rotation axis of the star, which can be described by a stream function or flux function

$$\Psi(r) = \frac{\mu}{r}\sin^2\theta \quad \text{or} \quad r = r_\mathrm{d}(\Psi)\sin^2\theta. \tag{14}$$

r_d is the radius from where the matter starts channeling along the magnetic field lines. By using these assumptions, from equations (10)–(12), we can obtain two relations (for more details, see Koldoba *et al*. 2002)

$$\frac{|\omega - \Omega|}{\Omega} \ll 1 \quad \text{and} \quad \frac{B_\phi}{B_p} \ll 1. \tag{15}$$

The first relation shows that angular velocity of matter is equal to the angular velocity of the field lines, i.e., matter and field lines are co-rotating. In addition to this, if there is no slippage between the lines and the star's surface, i.e., field lines are frozen into the star's surface, then we can equate $\Omega = \Omega_{\rm star}$. The second relation implies that the azimuthal component of the magnetic field B_ϕ is negligible as compared to the poloidal component of the magnetic field B_p, and hence we can neglect B_ϕ in our calculation.

2.3 *Bernoulli function*

The Bernoulli function (equation (13)) reduces to a simple form with the help of the above mentioned assumptions and the two relations in (15). Hence

$$\mathcal{B}(r, \rho) = \frac{v_p^2}{2} + h + \Phi_g(r) - \int \frac{Q\mathrm{d}r}{\rho v_p}, \tag{16}$$

where $v_p = [\mu\kappa(\Psi)(4 - 3r/r_d)^{1/2}]/(4\pi\rho r^3)$, h is the enthalpy, $r_{co} = \left(GM/\Omega^2\right)^{1/3}$ is the co-rotation radius, $\alpha = r_{co}/r_d$ is considered to be one in this paper and

$$\Phi_g(r) = -\Omega^2 r_{co}^2 \left(\frac{\alpha r_d}{r - r_g} + \frac{r^3}{2\alpha^2 r_d^3}\right).$$

The Equation of Motion (EoM) is given by

$$\frac{\partial \mathcal{B}}{\partial r} + \frac{\partial \mathcal{B}}{\partial \rho}\frac{\mathrm{d}\rho}{\mathrm{d}r} = 0 \ \text{ or } \ \frac{\mathrm{d}\rho}{\mathrm{d}r} = \frac{-\partial\mathcal{B}/\partial r}{\partial\mathcal{B}/\partial\rho}. \tag{17}$$

The flow starts with subsonic velocity at the r_d, but as matter moves toward the star, at some radius (say r_c), the flow becomes super-sonic. At that radius r_c, the numerator and denominator of EoM (17) become zero or $\frac{\partial\rho}{\partial r}|_{r_c} = \frac{0}{0}$. That is why r_c is also known as the critical radius or the critical point. However, $\frac{\partial\rho}{\partial r}|_{r_c} = \frac{0}{0}$ can be solved with L'Hospital's rule and we can obtain the solution by integrating the EoM from the critical point.

If there is no source or sink in energy equation, i.e., $Q = 0$ in equation (5), then we obtain the adiabatic relation by integrating it and obtain

$$p = \mathcal{K}\rho^\gamma, \tag{18}$$

where γ and $\mathcal{K}$ are the adiabatic index and measure of entropy, respectively. If we use the continuity equation (8) and replace ρ in terms of the sound speed, then we can write the entropy-accretion rate as $\dot{\mathcal{M}}$ for adiabatic flow

$$\dot{\mathcal{M}} = v_p A_p c_s^{2n} \quad \text{and} \quad n = \frac{1}{\gamma - 1}. \tag{19}$$

Here, $c_s = \sqrt{\gamma p/\rho}$ is the sound speed. Since, in this paper, we are considering the cooling processes, therefore $\dot{\mathcal{M}}$ is not constant along the flow.

2.4 *Shock conditions*

The shock conditions can be obtained from the conservation of fluxes, i.e. mass flux conservation, momentum flux conservation and total energy flux conservation (Kennel *et al*. 1989). If we use the strong magnetic field assumption and the two relations in equation (15), then MHD shock conditions reduce to hydrodynamics shock conditions but the information of magnetic field comes through the poloidal velocity and mass density. Therefore the shock conditions are

$$\begin{aligned}
&[\rho v_p] = 0,\\
&\left[\rho v_p^2 + p\right] = 0,\\
&\left[\rho v_p \frac{v_p^2}{2} + \rho v_p h - \rho v_p \int \frac{Q\mathrm{d}r}{\rho v_p}\right] = 0.
\end{aligned} \tag{20}$$

3. Methodology

To find an accretion solution, we need five input parameters. Out of the five parameters there are two main parameters, rotation period P of the star and density ρ_d at r_d radius. The third parameter is the star's surface magnetic field B_{po} which is related to rotation period of the star (Pan *et al*. 2013). The other two parameters are the mass and radius of the star. By using these input parameters in the critical point conditions which requires the numerator and denominator of EoM to be zero at the critical point, one can obtain the mathematical boundary condition of the equations of motion. The EoM (17) can be recasted as

$$\frac{\mathrm{d}v_p}{\mathrm{d}r} = \frac{N(r, v_p)}{D(r, v_p)}, \tag{21}$$

where, at $r = r_c$, or at the sonic point,

$$N = \frac{3c_{sc}^2}{2r_c}\left(\frac{8 - 5r_c/r_d}{4 - 3r_c/r_d}\right) - \frac{\delta}{n} - \Phi_g'(r_c) = 0$$

and

$$D = \left(v_{pc} - \frac{c_{sc}^2}{v_{pc}}\right) = 0.$$

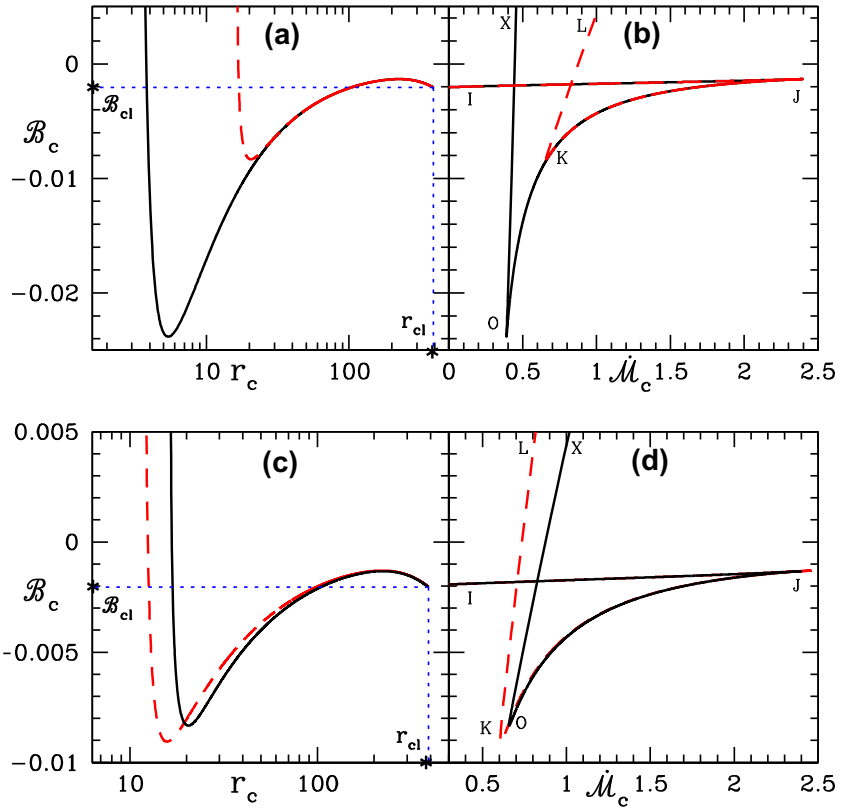

Figure 1. Total energy $\mathcal{B}_c$ is plotted with r_c **(a)** and **(c)**, and $\mathcal{B}_c$ vs. entropy accretion rate $\dot{\mathcal{M}}_c$ **(b)** and **(d)**. The plots are for two values of surface magnetic field: $B_{p\circ} = 10^9$ G (solid-black line) and 10^{11} G (dashed-red line) for a density of $\rho_d = 5.0 \times 10^{-10}$ g cm^{-3} (a, b). In (c) and (d), the plots are for two values of density: $\rho_d = 5.0 \times 10^{-10}$ g cm^{-3} (solid-black) and 1.0×10^{-8} g cm^{-3} (dashed-red line) for $B_{p\circ} = 10^{11}$ G. All the plots are for $P = 1$ s.

In the above,

$$\delta \equiv \frac{Q}{\rho v_{pc}}.$$

If we use the relation, $v_p = \mu\kappa(\Psi)\,(4 - 3r/r_d)^{1/2}\,/\,(4\pi\rho r^3)$ (because, $v_p = \kappa(\Psi)B_p/[4\pi\rho]$), then we can rewrite δ as

$$\delta \equiv \frac{4\pi\, Q r_c^3}{\mu\kappa\sqrt{4 - 3r_c/r_d}}.$$

By solving these equations, we can determine ρ_c (or v_{pc}) and T_c at r_c. The total energy can be obtained by plugging these variables in equation (16) and expressing $\mathcal{B}_c$ or $\mathcal{B}$ as a function of r_c. The density slope or velocity slope at the critical point is calculated by using the L'Hospital rule. In the strong gravity domain, the centrifugal force (due to non-zero angular momentum of matter) can modify the gravitational interaction and give rise to three types of critical points: spiral type (or middle critical point), inner critical point and outer critical point, which are X-type critical points. Suppose we have one X-type critical point (either inner or outer critical point) and we have values of all the variables at the critical point. Then we integrate the solution forward and backward from the critical point with fourth order Runga-Kutta method. We simultaneously check the shock conditions (21) in the supersonic branch. If they satisfy the shock conditions at some radius, we obtain shocked accretion solution. We calculate the post shock variables from these conditions and then start the integration from there. So the next step is to iterate the shock location to find a solution which satisfies the surface boundary conditions of the star. By using these methods, we have studied the parameter space and have found many consistent accretion solutions for different rotation periods of the star.

4. Results and discussion

An accretion disc with Keplerian angular momentum distribution, extending from large distance to the star surface is a possibility, however, in the presence of the magnetic field, this is a remote possibility. Matter

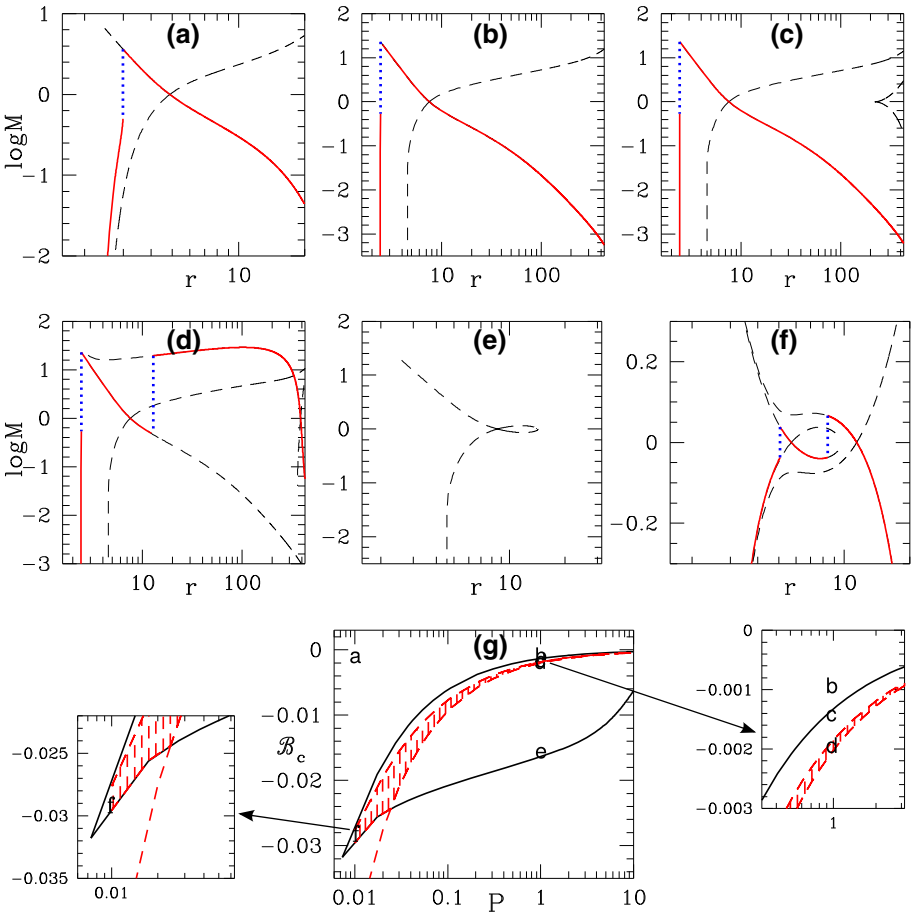

Figure 2. Mach number (M) versus r for six solutions **(a)–(f)**. Each panel corresponds to regions marked as (a)–(f) in $\mathcal{B}_c - P$ parameter space for MCP (solid bounded region in panel **(g)**). In panels (a)–(f), accretion solution is represented by solid-red line, shock by dotted-blue line and other branches of the solution by dashed-black line. In panel (g), region bounded by solid-black curve is the MCP region and the shaded-red region represents the multiple shock region. All plots are for $\rho_{\rm d} = 5 \times 10^{-10}$ g cm^{-3}.

would channel along magnetic field lines onto the poles. And the surface of the star at the poles will resist the supersonic flow. Therefore, an accretion onto a compact star with hard surface, is necessarily associated with a shock transition close to the star surface. In this paper, we discuss all possible accretion solutions in steady state, falling along the magnetic field lines under the assumptions made in section 2.2. All these solutions should terminate in a shock, In this paper, the analysis is done in geometrical units, which means that velocity is in units of c and distance in terms of $r_{\rm g} = 2GM/c^2$. We have considered the radius and mass of the star as $R_{\rm star} = 1.0 \times 10^6$ cm and $M = 1.4 M_\odot$, respectively. Therefore, in units of $r_{\rm g}$, the radius of the star is $R_{\rm star} = 2.418 r_{\rm g}$. Although, the analysis is done in geometric units, we quote the rotation period (P) in seconds, in order to provide a feeling of the rotation period of the star for the reader. As discussed in the methodology section, for a set of input parameters, basically the star rotation period P, $\rho_{\rm d}$ and $B_{\rm po}$, we can obtain mass density ρ_c, temperature $T_{\rm c}$ and $B_{\rm c}$ at the critical point. So, for $P = 1$ s and $\alpha = 1$, we have plotted $\mathcal{B}_{\rm c}$ versus $r_{\rm c}$ in Figures 1(a), (c) and $\mathcal{B}_{\rm c}$ versus $\dot{\mathcal{M}}_c$ in Figures 1(b), (d). In the upper two panels of Figures 1(a) and 1(b), we consider $\rho_{\rm d} = 5.0 \times 10^{-10}$ g cm^{-3}, but two values of the magnetic field $B_{\rm po} = 10^9$ G (solid-black line) and $B_{\rm po} = 10^{11}$ G (dashed-red line). In Figures 1(c) and 1(d), we consider the surface magnetic field as $B_{\rm po} = 10^{11}$ G, but two values of $\rho_{\rm d} = 1.0 \times 10^{-8}$ g cm^{-3} (solid-black line) and $\rho_{\rm d} = 5.0 \times 10^{-10}$ g cm^{-3} (dashed-red line). If there is a maximum and a minimum in the $\mathcal{B}_{\rm c} - r_{\rm c}$ curve for a given value of P, then there is a possibility of forming multiple critical points or MCP. The dotted lines in Figures 1(a) and 1(c) show the upper limit of $r_{\rm c}$, i.e., $r_{\rm cl}$ and its corresponding energy $\mathcal{B}_{\rm cl}$. Let us call the minimum(or maximum) in $\mathcal{B}_{\rm c}$ as $\mathcal{B}_{\rm c\,min}$(or $\mathcal{B}_{\rm c\,max}$), then for $\mathcal{B}_{\rm c\,max} > \mathcal{B} > \mathcal{B}_{\rm c\,min}$, the

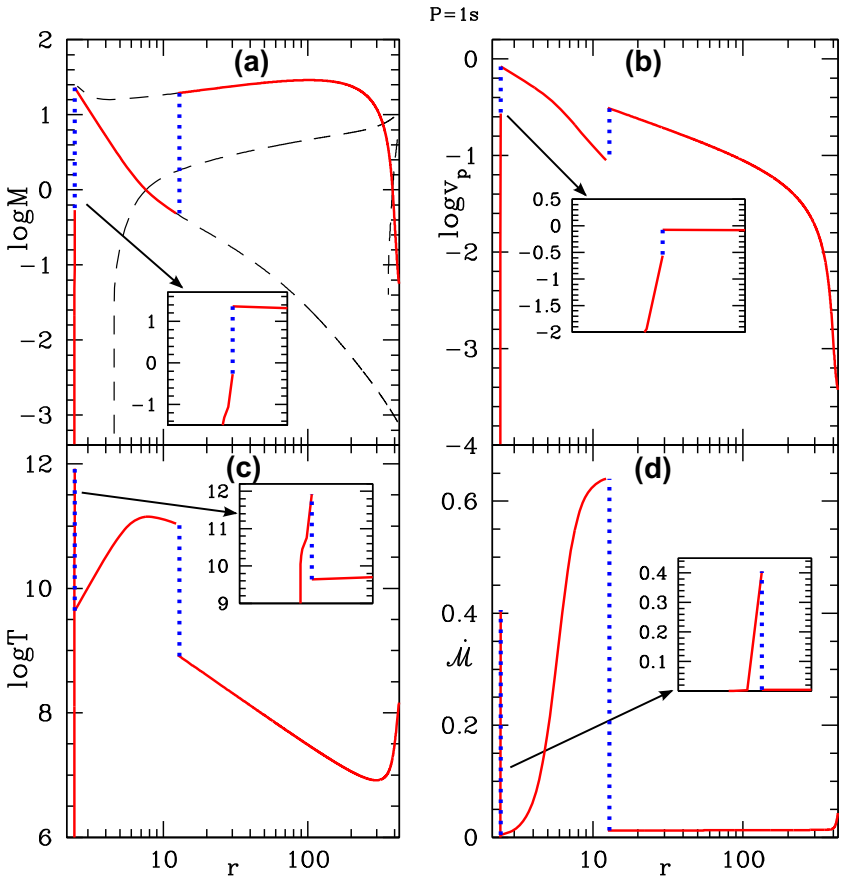

Figure 3. The accretion solution for $P = 1$ s and $B_{\rm po} = 10^{10}$ G. **(a)** M, **(b)** $v_{\rm p}$, **(c)** T and **(d)** $\dot{\mathcal{M}}$ as a function of r. The accretion solution is represented by solid-red line, shock by dotted-blue line and other branches of solution by dashed-black line. Accretion parameters are the same as in Fig. 2(d).

flow will harbour multiple sonic/critical points. But if $\mathcal{B}_{\rm c\,min} \leq \mathcal{B} \leq \mathcal{B}_{\rm cl}$, then there can only be two sonic points, where the inner one is X-type and the other one is the spiral type. The $\mathcal{B}_{\rm c}$–$\dot{\mathcal{M}}_{\rm c}$ plots (Figures 1(b) and 1(d)) also show the same effect. The kite-tail feature is symptomatic of MCP. Various combinations of $\mathcal{B}_{\rm c}$ and $\dot{\mathcal{M}}_{\rm c}$, produce sonic points: the LK (XO) branch of the dashed(solid) curve is the loci of the inner sonic points, the KJ(OJ) branch of the dashed(solid) curve is the loci of the middle sonic points and the IJ is the loci of the outer sonic points (Figures 1(b), (d)). As long as the entropy of the inner sonic point ($\dot{\mathcal{M}}_{\rm c}$) is greater than that of the outer sonic point, there is possibility of a second shock formation away from the star surface, in addition to the shock forming close to the star surface.

As has been pointed out, the accretion onto a compact star with hard surface should end with a shock very close to the surface. In this paper, we aim to study all possible accretion solutions in addition to this terminal shock near the star surface. The sonic point properties of Figures 1(a)–(d) appear similar to the black hole systems (Kumar & Chattopadhyay 2013, 2014, 2017; Chattopadhyay & Kumar 2016) although the inner boundary condition is quite different. However, unlike hydrodynamic studies in black hole system, in the strongly magnetized NS system, we find that $r_{\rm c} \leq r_{\rm cl}$. Observations also tell us that there exist a relation between period of rotation and the surface magnetic field (Pan *et al.* 2013). Thus, henceforth we consider a simple empirical relation inspired from the observations of Pan *et al.* (2013), and we assume it to be $B_{\rm po} = 10^{0.75 \log P + 10}$, where $B_{\rm po}$ and P is in Gauss and in seconds, respectively. If we now change P, we will get a set of $\mathcal{B}_{\rm c}$–$r_{\rm c}$ plots, each with its own extrema and $\mathcal{B}_{\rm cl}$. If all the maxima and minima are joined in the $\mathcal{B}_{\rm c} - P$ parameter space, we obtain a bounded region (solid curve) in Fig. 2(g). Any set of parameters in this bounded region will produce MCP for the accretion solution. The shaded region will produce the outer or the second shock. The lower bound of the shaded region is the loci of $\mathcal{B}_{\rm cl}$. Any point within the lower

bound of the shaded region and the lower bound of the MCP region will harbour two sonic points, the inner one being X-type and the outer one being spiral type. Any parameter set between the lower bound of the shaded region and the upper bound of the MCP region will harbour three sonic points, the inner and outer being X-types and the centre as a spiral type. We have marked locations on the $\mathcal{B}_c - P$ parameter space as 'a'–'f', and then plotted the corresponding solutions in terms of the Mach number $M = v_p/c_s$ as a function of r, in Figures 2(a)–(f), named after the location of the corresponding coordinates in Fig. 2(g). The accretion solutions are represented by solid-red lines, the shock is denoted by dotted-blue lines and other branches of solutions are represented by dashed-black lines. Figure 2(a) corresponds to high energy ($\mathcal{B}_c = 0.001$) and low rotation period ($P = 10$ ms), the accretion flow becomes transonic through the inner sonic, and goes very close to the star surface and undergoes a shock transition. The next solution is Fig. 2(b) plotted for accretion parameters $\mathcal{B} = \mathcal{B}_c = 0.001$ and $P = 1$ s which lies outside the bounded region or the MCP region (solid-black line). This solution is similar to the previous one. The third solution is Fig. 2(c), for parameters $P = 1$ s and $\mathcal{B} = \mathcal{B}_c = 0.0015$ which lies just inside the MCP region (see inset to Fig. 2(g)). Therefore in Fig. 2(c), we have one solution which passes through the inner critical point and the other is the cusp type solution through the outer critical point (dashed). Therefore the flow becomes transonic after crossing the inner sonic point and suffers only one shock near the star surface. Figure 2(d) is the solution for $P = 1$ s and $\mathcal{B}_c = 0.00203$ which lies in the multiple shock region (shaded-red region). Therefore, in this case, flow first passes through the outer critical point and becomes super-sonic. Then it forms a shock transition just before the inner critical point, then it passes through the inner critical point and form another shock near the star surface to satisfy the surface boundary conditions. The solution in Fig. 2(e) is situated below the lower bound of the dashed region i.e., $\mathcal{B} < \mathcal{B}_{cl}$ and therefore shows an inverted α type solution. Since this is not a global solution, no accretion is possible. In this case, we have only two critical points: one is X-type and the other is spiral type but we do not have an outer critical point. In all the above cases, the X-type sonic points are those where the accretion and wind type solutions cross, while the solutions skirt the spiral type sonic point. The last solution is Fig. 2(f), for rotation period $P = 10$ ms which is the same as that in Fig. 2(a), but lies inside the multiple shock region (shaded-red). In this case also, the flow has double shock, similar to the solution in Fig. 2(d).

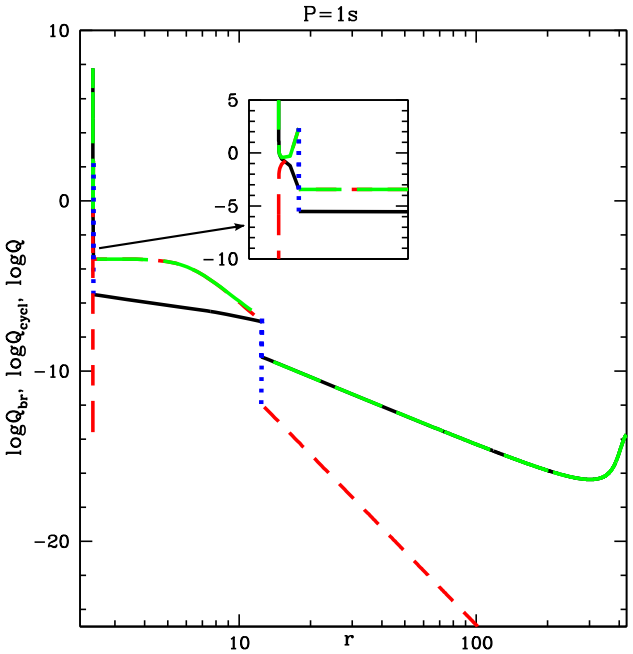

Figure 4. Variation of emissivity of different radiative processes Q_{br} (solid, black), Q_{cycl} (dashed, red) and total cooling Q (long-dashed, green) which corresponds to the solution as in Figures 3(a)–(d).

However in this case, the solution which passes through the inner critical point is alpha type.

We have plotted the Mach number M (Fig. 3(a)), poloidal velocity v_p (Fig. 3(b)), temperature T (Fig. 3(c)) and entropy-accretion rate ($\dot{\mathcal{M}}$) (Fig. 3(d)) as a function of r. The accretion parameters are $P = 1$ s, $B_{po} = 10^{10}$ G, $\rho_d = 5 \times 10^{-10}$ g cm^{-3} and $\mathcal{B} = 0.00203$ (similar to Fig. 2(d)). The accretion flow passes through the outer sonic point and then suffers a shock at $12.897 r_g$. The subsonic post-shock matter accelerates and again becomes supersonic as it crosses the inner sonic point. This supersonic matter again suffers a shock at $2.434 r_g$, which is very close to the surface of the star. The inset in each panel zooms the inner shock. The temperature and the poloidal velocity starts at low values and becomes relativistic. The temperature in the inner post-shock disc reaches to a very high values, only decrease drastically down to very low values. Because of the presence of cooling, the entropy is not constant (Fig. 3(d)).

In Fig. 4, we plot the emissivity of different cooling processes with r for the accretion solution depicted in Figures 3(a)–(d) for $P = 1$ s. Different curves represent the bremsstrahlung Q_{br} (solid, black), cyclotron Q_{cycl} (dashed, red) and the total emissivity Q (long-dashed, green). At larger distance, the cooling process is dominated by bremsstrahlung, while in the post-shock region and near the surface, cyclotron process dominate. The

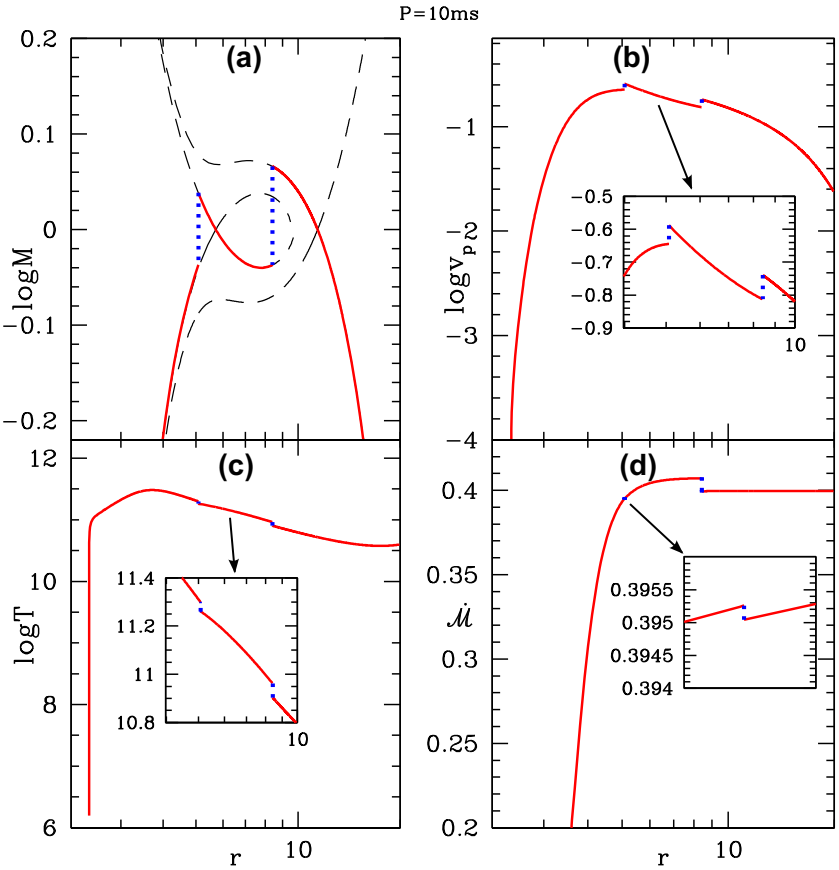

Figure 5. Variation of **(a)** $\log(M)$, **(b)** $\log(v_{\rm p})$, **(c)** $\log(T)$ and **(d)** $\dot{\mathcal{M}}$ with r. Accretion solution (solid, red), shock jump (dotted, blue) and other branches (dashed, black) are shown. Other parameters are $P = 10$ ms and $\rho_{\rm d} = 5 \times 10^{-10}$ g cm^{-3}.

cooling rate close to the surface overwhelms and both T and $v_{\rm p}$ plummets several orders of magnitude. The inset shows the cooling rates in the post-shock region close to the star surface.

We plot M (Fig. 5(a)), $v_{\rm p}$ (Fig. 5(b)), T (Fig. 5(c)) and $\dot{\mathcal{M}}$ (Fig. 5(d)), which also harbours multiple shock with a much faster rotating system with $P = 10$ ms, $B_{\rm p\circ} = 3.16 \times 10^8$ G and $\rho_{\rm d} = 5 \times 10^{-10}$ g cm^{-3}. This is the same solution as is depicted in Fig. 2(f). The two shocks are located at 5.081 and 8.414, but are much weaker than the previous case.

In Figures 3(a)–5(d), we have discussed two solutions with high and low spin periods, which become transonic at two places and harbour multiple shocks. Now, we look into two solutions once again for high and low periods, but which become transonic only at one place, and harbour one shock close to the star surface. As a representative case, we consider the two solutions depicted in Figures 2(a) and (b) characterized by spin period $P = 10$ ms and $P = 1$ s respectively, but with the same Bernoulli parameter $\mathcal{B}$. In Fig. 6(a), we plot the poloidal velocity $v_{\rm p}$ and temperature T for $P = 10$ ms in the log scale. In Fig. 6(b), we plot the poloidal

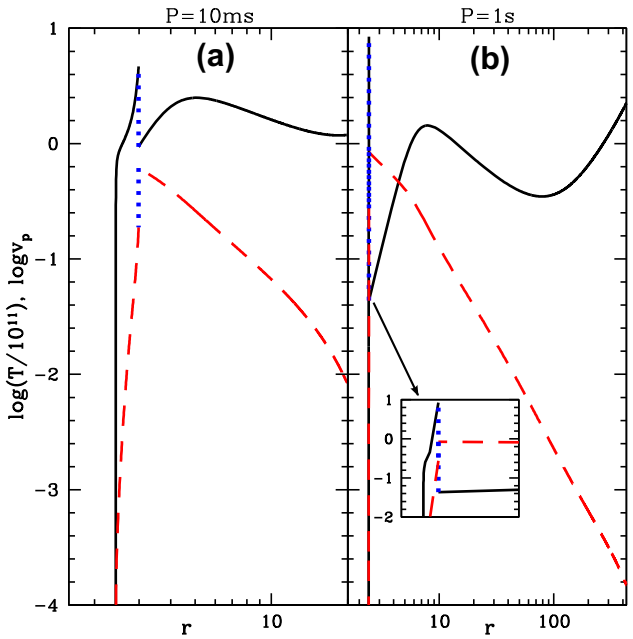

Figure 6. Accretion solutions $\log(v_{\rm p})$ (dashed, red) and $\log(T)/10^{11}$ (solid, black) for $P = 10$ ms **(a)** and $P = 1$ s **(b)**. Other accretion parameters are $\mathcal{B} = 0.001$ and $\rho_{\rm d} = 5 \times 10^{-10}$ g cm^{-3}.

velocity v_p and temperature T for $P = 1$ s in the log scale. In both the cases, the shock is at $3r_g$, which is just outside the star surface, but the post-shock temperature is higher for the slowly rotating star. The cyclotron radiation in the post-shock region is quite strong and drastically reduce both v_p and T, such that it satisfies the inner boundary condition of $v_p(R_{star}) \sim 0$.

5. Conclusion

In this paper, we have studied the magnetized accretion solutions which have one or two shocks for different rotation periods of the star, including cooling mechanisms (bremsstrahlung and cyclotron) in the Paczyński–Wiita potential. From our study of the MCP parameter space, for a range of rotation period (few ms–10 s), we find that there is a lower limit on the rotation period P_{min} below which MCP is not possible, and so we cannot have multiple shocks. Therefore, for accreting NS cases, where spin period is low, e.g., SAX J1808.4-3658 with $P = 2.41$ ms, there can be only one shock very close to the star surface.

We find correct accretion solutions with cooling mechanisms (bremsstrahlung and cyclotron cooling) for different rotation period, $P = 10$ ms and 1 s. Depending on the energy of the flow, accretion solutions may have one or two stationary shocks. If two shocks are present, then the outer shock is at a radius of $\sim 10r_g$ and the inner shock is at a radiusof $\sim 3r_g$, else, only one shock is present very close to the surface. One has to consider cooling mechanism, otherwise, either the velocities are too high close to the star surface (Koldoba *et al*. 2002) or the shocks are much further away than what observations suggest.

Our results show that cooling processes dominate near the star. We found that bremsstrahlung emission dominates at larger distance, as well as near the star surface, while cyclotron cooling dominates in a region closer to the star. In black hole system, it has been noted that the bremsstrahlung process is an inefficient cooling process, while in the present NS case, we found this process to be quite effective. The simple reason is that the cross-section of accretion onto a black hole is spherical (i.e., $\propto r^2$, matter crosses the horizon with c), while for NS the cross-section or A_p is dictated by the magnetic field configuration. Now, dA_p/dr for a dipole magnetic field increases sharper than that of the spherical cross-section, which makes flow near the NS surface to be denser. This makes bremsstrahlung stronger for the NS case. As the result of the presence of cooling processes, all the solutions in this paper satisfy $v_p \lesssim 10^{-8}c$ close to the star surface. We must however accept that, since the rotation axis and magnetic axis are aligned in the present analysis, it can only make qualitative assessment of pulsars. This analysis is more suited to address accreting NS system which have weak pulsations or none at all.

These accretion solutions with cooling mechanisms are able to connect the flow from the disc to the star surface via shock/shocks. We find that cyclotron cooling is necessary along with bremsstrahlung cooling to find plausible accretion solutions. These solutions should help explain the accretion process and radiation mechanisms of accreting NSs.

References

Busschaert C., Falize E., Michaut C., Bonnet-Biadaud J. M., Mouchet M. 2015, A&A, 579 A, 25

Camenzind M. 1990, Rev. Mod. Astron., 3, 234

Chattopadhyay I., Chakrabarti S. K. 2002, MNRAS, 333, 454

Chattopadhyay I., Kumar R. 2016, MNRAS, 459, 3792

Das S., Chattopadhyay I. 2008, New. Astron., 13, 549

Davidson K., Ostriker J. P. 1973, ApJ, 179, 585

Ghosh P., Lamb F. K. 1979, ApJ, 232, 259

Heinemann M., Olbert S. 1978, J. Geophys. Res., 83, 2457

Karino S., Kino M., Miller J. C. 2008, ApJ, 119, 739

Kennel C. F., Blandford R. D., Coppi P. 1989, J. Plasma Physics, vol. 42, part 2. pp. 299–319

Koldoba A. V., Lovelace R. V. E., Ustyugova G. V., Romanova M. M. 2002, AJ, 123, 2019

Kumar R., Chattopadhyay I. 2013, MNRAS, 430, 386

Kumar R., Chattopadhyay I. 2014, MNRAS, 443, 3444

Kumar R., Chattopadhyay I. 2017, MNRAS, 469, 4221

Lamb F. K., Pethick C. J., Pines D. 1973, ApJ, 184, 271L

Li J., Wilson G. 1999, ApJ, 527, 910

Lovelace R. V. E., Mehanian C., Mobarry C. M., Sulkanen M. E. 1986, ApJ, 62, 1

Lovelace R. V. E., Romanova M. M., Bisnovatyi-Kogan G. S. 1985, MNRAS, 514, 368

Ostriker E. C., Shu F. H. 1995, ApJ, 447, 813

Paatz G., Camenzind M. 1996, A&A, 308, 77 p.

Pan Y., Zhang C., Wang N. 2013, Proceedings of the International Astronomical Union, IAU Symposium, Volume 290, pp. 291–292

Pringle J. E., Rees M. J. 1972, A&A, 21, 1

Ustyugova G. V., Koldoba A. V., Romanova M. M., Chechetkin V. M., Lovelace R. V. E. 1999, ApJ, 516, 221